HAL open science

An extensive numerical study of the burning dynamics of wildland fuel using proposed configuration space

Kai Zhang, Aymeric Lamorlette

To cite this version:

Kai Zhang, Aymeric Lamorlette. An extensive numerical study of the burning dynamics of wildland fuel using proposed configuration space. International Journal of Heat and Mass Transfer, 2020, 160, pp.120174. 10.1016/j.ijheatmasstransfer.2020.120174 . hal-03232086

HAL Id: hal-03232086

https://hal.science/hal-03232086v1

Submitted on 21 May 2021

HAL is a multi-disciplinary open access archive for the deposit and dissemination of scientific research documents, whether they are published or not. The documents may come from teaching and research institutions in France or abroad, or from public or private research centers.

L'archive ouverte pluridisciplinaire **HAL**, est destinée au dépôt et à la diffusion de documents scientifiques de niveau recherche, publiés ou non, émanant des établissements d'enseignement et de recherche français ou étrangers, des laboratoires publics ou privés.

An extensive numerical study of the burning dynamics of wildland fuel using proposed configuration space

Kai Zhang*, Aymeric Lamorlette

M2P2, Aix-Marseille University, CNRS. 38 rue Joliot-Curie, Centrale Marseille Plot 6 13451 Marseille, France

ARTICLE INFO

Article history:
Received 6 February 2020
Revised 26 June 2020
Accepted 6 July 2020
Available online 15 July 2020

Keywords:
Heat transfer
Forestfirefoam
Flame model
CFD
Porous
Combustion

ABSTRACT

Physics-based flame models capable of predicting small-scale fire behaviors reduce computational power needed for predicting fires of large- and giga-scale. However, classical model correlations are often developed for 'free fires' without considering vegetation around. These models may result in inaccurate fire modeling due to wrong 'prior' flame shape estimated from θ ~ wind speed. To overcome this defect, three-dimensional small-scale fires with fireline intensity of 100 KW/m are numerically simulated using large eddy simulation. Fire behaviors such as flame tilt angle and heat transfer mechanisms are extensively studied using a newly proposed configuration space $\{N_C, CdLAI\}$. The former one represents the ratio between fire to wind power, and the latter one considering the vegetation effect is for the first time introduced in flame models. Using the configuration space, two model correlations for flame tilt angle and radiative heat power reaching the unburnt fuels are proposed. The flame tilt angle θ is directly related to $CdLAI$ ($C_d\alpha_s\sigma_s H_F/2$), while inversely related to N_C ($2gI/\rho_0 C_{p,0} T_0 U_0^3$), in contrast to the model proposed for radiative heat power. Comparisons with several classical models evidenced the capability of new flame models in predicting both free and non-free fires. The limits of the validity of the newly proposed models are also discussed.

1. Introduction

The burning behavior of wildland fuels represents one of the very complex heat and mass transfer problems because it is greatly affected by many physical parameters such as the characteristics of vegetation, the topography, and the environmental conditions [1]. All of these parameters have potentially influenced the mass, momentum, and energy (heat) exchanges between the solid fuel particles and the surrounding atmosphere. As a result of these mutual exchanges, fire regime transition and its associated heat transfer mechanisms emerge as two primary factors co-controlling the burning dynamics of wildland fuels. Depending on dimensionless numbers such as Froude (F_C), squared Froude (F_C^2) or Byram convective number (N_C) [2,3], wildland fires are often classified into two regimes: a plume-dominated regime and wind-driven regime. For plume-dominated fire, radiative heat transfer dominates to the fire front propagation whereas for wind-driven fire, both radiative and convective heat transfer contributes to the ignition of unburnt fuels.

Nelson [4] analysed previous experimental data of Morandini and Silvani [5] based on a triangular flame model and an alternative way to define flame height and tilt angle. The flame height defined F_C^2 (denoted as F_{CH}^2) best described the mode of heat transfer to unburnt fuels. The other two potential indicators of fire regime transition and heat transfer mechanism are flame height defined F_C (denoted as F_H) and the N_C. For $N_C < 2$, a wind-driven fire with large tilt angle is dominated by convective heat transfer; for $N_C > 10$, a plume-dominated fire with tilt angle smaller than 20° is governed by radiation. A mixed heat transfer mechanism occurs when $2 < N_C < 10$. These analyses are in agreement with that reported by Morvan and Frangieh [6] in whose work selected data of laboratory fires at various experimental conditions are re-visited.

Although the burning dynamics of wildland fires have been broadly discussed in the literature [7–12] using N_C ($2gI/\rho_0 C_{p,0} T_0 U_0^3$), the role of this dimensionless number is questioned from a physical point of view especially for small-to-medium scale fires. In 2015, Lamorlette et al. [13] discussed the relevance between several dimensionless numbers and the cylindrical type particle (solid fuel) ignition time $t_{s,\,ig}$. Amongst several dimensionless numbers such as the Prandtl number Pr, the radiative Biot number Bi [14], the particle quasi-static Reynolds number Re_{σ_s} and the Nusselt number N_u, only two parameters were identified most relevant for solid fuel ignition under natural convection:

* Corresponding author.
E-mail addresses: kai.zhang.1@city.ac.uk (K. Zhang), aymeric.lamorlette@univ-amu.fr (A. Lamorlette).

Nomenclature

Bi	Biot number
C_d	Drag coefficient
$C_{p,0}, C_{p,s}$	Specific heat capacity for ambient air and solid ($\mathrm{Jkg^{-1}K^{-1}}$)
D	spanwise width of burner/flame (m)
D_0	flame depth (m)
F_C	Froude number
F_D	Drag force (N)
g	Gravitational acceleration ($\mathrm{ms^{-2}}$)
ΔH_C	heat of combustion ($\mathrm{Jkg^{-1}}$)
H_F	Vegetation height (m)
H_{flame}	Height of flame (m)
h, h_T	Heat transfer and total heat transfer coefficient ($\mathrm{Wm^{-2}K^{-1}}$)
I	Fireline intensity (KW)
J	Irradiance ($\mathrm{Wm^{-2}}$)
LAI	Leaf area index, $\alpha_s \sigma_s H_F/2$
$\dot{m}''$	mass burning rate per unit area (mass flux) ($\mathrm{kgm^{-2}s^{-1}}$)
N_u	Nusselt number
N_C	Byram convective number, $2gI/\rho_0 C_{p,0} T_0 U_0^3$
Pr, Pr_t	Prandtl and turbulent Prandtl number
R_i	Richardson number
Re, Re_d, Re_{σ_s}	Reynolds, particle Reynolds and quasi-static Reynolds number.
s	Stochiometric fuel/oxygen mass ratio
T, T_s, T_0, T_f	Gas, solid, ambient, and flame temperature (K)
$T_{ig}, T_{s,\,ig}$	Gas and solid ignition temperature (K)
U_0, U_e	Wind speed, entrainment velocity ($\mathrm{ms^{-1}}$)
w_0	Characteristic buoyancy velocity ($\mathrm{ms^{-1}}$)
w_{flame}	Width of flame (m)
Greek symbols	
α_g, α_s	Volume fraction of gas and solid
σ	Stefan-Boltzmann constant
σ_s	Surface to volume ratio (SVR) ($\mathrm{m^{-1}}$)
μ, ν, ν_t	Dynamic, kinematic, and turbulent kinematic viscosity
$\tau_{react}, \tau_{res}, \tau_k$	Chemical reaction, fire residence, and kernel characteristic time (s)
λ_s	Solid thermal conductivity ($\mathrm{Wm^{-1}K^{-1}}$)
ϕ_{surf}	Surface heat flux ($\mathrm{KWm^{-2}}$)
η	fraction of impinging air
ρ, ρ_0, ρ_s	Gas, ambient air, and solid density ($\mathrm{kgm^{-3}}$)
δ_{ij}	Kronecker delta
θ	Flame tilt angle (degree)

the $CdLAI(C_d \alpha_s \sigma_s H_F/2)$ and the ψ $(\alpha_s^2 \upsilon^2/gH_F)$. The former one accounts for induced momentum and in-depth radiation effects, and the latter one represents an induced sublayer hydrodynamic effect.

Apart from these two parameters, the minor effect of Re_{σ_s} was also highlighted. Within the fuel layer, the $\psi = \alpha_s^2 \nu^2/gH_F$ and $T_b^* = (T - T_0)/T$ together defined particle Reynolds number $Re_{\sigma_s} = \sqrt{1/\varphi CdLAI(T - T_0)/T}$. By roughly considering that ignition occurs at $T_b^* = 0.5$ and fuel ignition temperature $T_{s,\,ig}$ equals to the surrounding temperature T_{ig}, *i.e.*, $T_{s,\,ig} \sim T_{ig}$, a physical limit of $(CdLAI)_{lim} = 2 \times 10^{-6}$ was obtained that away from this value, Re_{σ_s} effect on the particle ignition time $t_{s,\,ig}$ is negligible. This is because away from the limit, sublayer flow is far from the point of vortex shedding transition [15,16] at which heat transfer from gas to solid phase (and hence $t_{s,\,ig}$) is modified. In the present study, because ψ is roughly 0.027 and $0.01 \leq CdLAI \leq 0.5$, giving $\psi CdLAI \gg 2 \times 10^{-6}$, the particle quasi-static Reynolds number has negligible influence on the fuel particle ignition time.

Therefore, the only two dimensionless numbers which affect the fuel particle ignition by heat transfer are indeed the $CdLAI$ and ψ. Because ψ accounts for induced sublayer flow, its effect can also be replaced by a Byram convective number N_C, which measures the competition effect between wind and fire power. The N_C is known to control fire behaviours such as the rate of spread, mass loss rate, flame residence time, heat transfer mechanism *etc.* in cases when an external forced flow exists [17–19]. To show the relevance between ψ and N_C, one may start with how N_C $(2gI/\rho_0 C_{p,0} T_0 U_0^3)$ is defined. This parameter modifies sublayer flow by imposing an atmospheric boundary layer (ABL) via an implicit wind speed dependency on Y_0 and H_F. The former is the burnt fuel roughness layer and the latter is the vegetation height, *i.e.*, $N_C \sim {Y_0}^{-1} \sim {H_F}^{-1}$. It can be used to replace ψ because it has similarities to $\psi = \alpha_s^2 \upsilon^2/gH_F$ that $\psi \sim H_F^{-1}$as well. Moreover, the intermediate relationship of $N_C \sim {Y_0}^{-1}$, with Y_0 approximately three times the H_F, is affected by Kelvin-Helmholtz instability [20] that the relevant turbulent length scale l_T is also strongly related to H_F [21,22].

As a result of above observations, it is reasonable to conclude that fire global behaviors are not solely dependent on N_C, but are governed by a configuration space $\{N_C, CdLAI\}$. These two parameters are internally coupled to affect local fuel ignition time by heat and mass transfer. However, none of previous studies has tried to correlate fire regime transition and heat transfer mechanism with this configuration space, *i.e.*, previous flame model was only built based on N_C alone. An accurate small- to medium-scale flame model considering the role of vegetation characteristics $CdLAI$ is essential to extend the limit of validity of large-scale fire models.

Furthermore, the importance and relevance of this new configuration space $\{N_C, CdLAI\}$ on solid fuel burning behavior can also be explained by the fact that fire global behavior has a dependency on two kinds of flows: an atmospheric boundary layer flow and a mixing layer flow. Ahead of the fire propagating front, the boundary layer to mixing layer transition occurs roughly at $CdLAI = 0.1$ [23], whereas behind the fire propagating front, ash layer modified atmospheric boundary layer effect [24] is non-ignorable and is implicitly governed by N_C,. The local fuel ignition time and global fire behaviors are hence a result of the competition between two kinds of flows governed by the configuration space $\{N_C, CdLAI\}$. It was observed by Lamorlette et al. [13] that for fire under no-wind condition with near zero rate of spread, the sublayer smouldering or pyrolysis process is influenced solely by $CdLAI$, while the coupling effect of N_C and $CdLAI$ remain unclear.

Overall, this study is motivated by the lack of understanding of the effect of configuration space $\{N_C, CdLAI\}$ on controlling the burning dynamics of the wildland fuels via the two key factors: the fire regime transition and the heat transfer mechanism. As far as the authors are aware, the only work which has discussed the effect of LAI, similar as $CdLAI$, on the fire regime transition is the one by Morvan and Lamorlette [25]. They reported that for a plume-dominated fire under moderate wind speed ($N_C \sim 23$), LAI has a notable influence on the amount of radiation reaching the unburnt solid fuel. With LAI increasing from 0.35 to 4.2, fuel temperature ahead of flame front approaches the gas temperature indicating an extra contribution of radiative heat transfer. This may suggest that the effect of canopy is to prevent the fire regime transition from plume-dominated to wind-driven. Studies based on different N_C and $CdLAI$ need to be performed to advance the knowledge of the wildland fuels burning behaviors and promote the basic understanding of heat and mass transfer across the vegetation.

This paper is organized as follows. Section 2 describes the 3D numerical configuration of the representative fire and introduces the mathematical models employed for the simulation.

Section 3 discusses the fire behaviors under different N_C and *CdLAI* values which compose the configuration space {N_C, *CdLAI*}. Finally, conclusions of the present study are given in Section 4.

2. Methods

2.1. Numerical details

In this study, 3D small-scale wildfires stabilizing on vegetation layers of different characteristics (*CdLAI*) are numerical simulated using an inert vegetation version of a compressible solver ForestFireFoam (FFF), an extension of FireFoam solver developed at M2P2 lab, Aix-Marseille University. It was previously demonstrated that the multiphase solver FFF is able to capture wildland fire behaviors in both no-wind and wind conditions with the sub-model improvements [26,27]. The inert version FFF solver is primarily based on the standard Gaussian finite-volume integration method and assumes an inert vegetation layer without considering the processes such as pyrolysis, char combustion, *etc.* to simplify the analysis. To represent the key processes for wildland fire, a burner is used to inject CO into the computational domain to mimic the main product of pyrolysis and char oxidation. The gas phase chemical reaction rate is then driven by the competition between the CO–air turbulent and molecular diffusion rates, *i.e.*, an improved model based on Eddy Dissipation Concept [28].

For high-wind speed induced wall-bounded flames, a wall-adaptive local eddy-viscosity (WALE) model is employed to return the correct wall asymptotic behavior [29] and to calculate the turbulent diffusion rate by solving an improved sub-grid scale kinetic energy equation [30]. The solid fuel temperature is essentially governed by both convective and radiative heat transfer from the gas phase, while an imposed cold gauge of Ts=295 K on the vegetation layer prohibits the solid temperature to increase for the purpose of measuring surface heat flux. The radiative intensity I_{rad} obtained from solving radiative heat transfer equations using a discrete ordinate method (fvDOM) [31] is integrated for a finite number of solid angles in order to calculate the total irradiance J from which the radiative source term Q^s_{rad} is defined by considering the radiation extinction coefficient $\alpha_s\sigma_s/4$ for convex particles [32]. Detail descriptions of the employed models are available in [26,27].

The computational domain is 7.8 m long in the streamwise x-direction, 2.5 m high in the vertical y-direction and 0.5 m wide in the spanwise z-direction partially given in Fig. 1. A vegetation layer of 5 m long, 0.05 m high and 0.5 m wide is imposed from the leading edge of the CO burner sitting at $x = 0.0$ m. For the present study, a small-scale fireline intensity of $100KW/m$ corresponding to a CO injection velocity of 0.173636 m/s and the burner size $0.05 \times 0.5m^2$ is used. Periodic boundary conditions are applied on the walls in the spanwise direction to reduce the required computational power without losing too many 3D flame front features of wildfires [33] such as the flame tower induced convective heating/cooling of solid particles [34]. A trip wire of 0.005 m long, 0.5 m wide and 0.005 m high is placed at x= $(-0.105)m$ to perturb the incoming boundary layer flow given by,

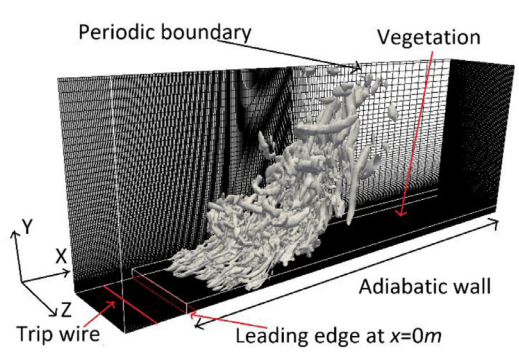

Fig. 1. Visualization of the computational domain using instantaneous isocontour of Q-criterion at 150 s^{-2}, clipped to $x_{max} = 2.5$ m, $y_{max} = 1$ m.

$$U_\infty(Y) = A \times U_{ref} \times ln\left(\frac{Y + Y_0}{Y_0}\right) \tag{1}$$

Where the surface roughness Y_0 is approximated as one tenth of the vegetation height $H_F = 0.05$ m to mimic the ashes left from burning wildland fuels [35]. The constant A is calculated using an open wind speed often defined at 10 m reference height [36,37],

$$U_{10}\left(Y = Y_{ref} = 10m\right) = A \times U_{10} \times \ln\left(\frac{Y}{Y_0} + 1\right); A = 0.1315546732 \tag{2}$$

To accurately capture the in-depth radiation and the ABL/canopy turbulence, the grid spacing used along streamwise x-direction is 0.005 m for x<1.0 m (main flame region) and vertical y-direction is 0.002 m on average for y<0.05 m, smaller than the cell size (Δ) requirement following the criterion [10],

$$\Delta < \min\left(\frac{H_F}{3}, \frac{2H_F}{LAI}\right) = \min(0.0167\,\text{m}, 0.02\,\text{m}) \tag{3}$$

With $0.1 \leq LAI \leq 5$ for the present study.

Considering the overall expansion ratio of the mesh in the less important plume regions responsible for little radiation, the total number of cells is 3.5 million with more details available in [12]. Statistical data is collected using the last 15 s out of 30 s of the total simulation time. The Courant–Fredrichs–Lewy (CFL) number [38] is restricted to be smaller than 0.5 using automatic time step adjustment. Each simulation requires CPU time of about 2500 h using 48 processors on high-performance computing (HPC) cluster of Aix-Marseille University.

2.2. The cold gauge, inert vegetation assumption

Because of the high computational power required for investigating the 3D propagating wildland fire behaviors, the present study assumes an inert vegetation on which a cold gauge of T_s = 295 K is imposed to measure the radiative heat transfer from the stationary fire body confined by $T = 500$ K. As mentioned above, a detail description of the chosen sub-models is available in [26,27], while the inert version FFF does not take evaporation, pyrolysis and char oxidation rates into account leading to the following T_s equation:

$$C_{p,\,s}\alpha_s\sigma_s\frac{dT_s}{dt} = Q^s_{rad} + Q^s_{conv} \tag{4}$$

The equation indicates that the time evolution of solid temperature (energy balance) is controlled by heat transfer between gas and solid via radiation $Q^s_{rad} = \alpha_s\sigma_s/4 \times (J - 4\sigma T_s^4)$ and convection $Q^s_{conv} = h\alpha_s\sigma_s \times (T - T_s)$.

Despite the ease of retrieving radiative heat transfer from $J \approx 4Q^s_{rad}/\alpha_s\sigma_s$, the cold gauge, inert vegetation assumption [39] brings a question of to what extent does the $T_s = T_0 \sim 295K$ influence the fire dynamics compared to that of a propagating fire. In a real propagating case, the heat flux reaching the vegetation is responsible for the solid temperature elevation and decomposition of the fuel following the three steps: evaporation, pyrolysis, and smouldering [40–42]. The evaporation process can be neglected considering the chosen dead pine needles as fuel, *i.e.,* zero fuel moisture content, while the pyrolysis and smouldering rates may be influenced by the cold vegetation assumption since solid temperature is not allowed to rise. In fact, without imposing the cold gauge, the inert vegetation temperature will finally rise to the fluid temperature $T_s = T \sim 1900$ K for a stationary flame, equivalent to a quasi-static propagation fire, *i.e.*, at any time during propagation, the vegetation is at steady-state. Neither the cold nor the hot vegetation

Table 1
Relevant parameters for calculation.

α_s	σ_s (m^{-1})	H_F (m)	C_d	$CdLAI$
$5.33 \times 10^{-4} \sim 2.66 \times 10^{-2}$	7500	0.05	0.1	0.01–0.5
ρ_s $(\mathrm{kgm^{-3}})$	$C_{p,s}$ $(\mathrm{Jkg^{-1}K^{-1}})$	h_T $(\mathrm{Wm^{-2}K^{-1}})$	λ_s $(\mathrm{Wm^{-1}K^{-1}})$	$T_{s,ig}$ (K)
831.7	2069.7	10–20	0.12	600

case may be representative of a real propagating fire without considering the competition between the fire residence time τ_{res} and the solid particle reaction time τ_{react}.

For $\tau_{res} \ll \tau_{react}$: vegetation has no time to adapt to the propagation of the flame front and it is reasonable to assume $T_S = T_0 \sim 295\,\mathrm{K}$ until ignition occurs, equivalent to a cold vegetation case.

For $\tau_{res} \gg \tau_{react}$: vegetation has enough time to reach steady-state $T_S = T \sim 1900\,\mathrm{K}$ before the flame front moves leading to a quasi-static propagation fire, equivalent to a hot vegetation case.

Following the study of Burrows [43], the fire residence time for a round wood particle having $\sigma_s = 7500\,\mathrm{m^{-1}}$ can be calculated as,

$$\tau_{res} = \frac{208487}{\sigma_s^{1.236}} \approx 3.4\,\mathrm{s} \tag{5}$$

In terms of solid fuel chemical reaction time, the best representation may be the characteristic time of a thermal kernel according to the study of Lamorlette and Candelier [44]. The Biot number $B_i = h_T L/\lambda_s$ and the dimensionless number $\varphi = \phi_{surf} L/\lambda_s (T_{s,ig} - T_0)$ co-determine the validity of either the thermally thick or thermally thin approach. For the present study, the total heat transfer coefficient h_T, which considers both convection and radiant-emission ranges from 10 to 20 $\mathrm{Wm^{-2}K^{-1}}$ according to several studies [45–47], the characteristic length $L = 2/\sigma_s = 2.67 \times 10^{-4}\mathrm{m}$, the solid heat conductivity $\lambda_s = 0.12\,\mathrm{Wm^{-1}K^{-1}}$ and the solid ignition temperature $T_{s,ig} \approx 600\,\mathrm{K}$. In the solver, a suited Nusselt correlation is used to calculate the h_T, while radiation is fully resolved as explained in [26,27]. The value of h_T=10–20 $\mathrm{Wm^{-2}K^{-1}}$ is then chosen only to evaluate B_i and the solid chemical reaction time. With the $\phi_{surf} \approx 42\,\mathrm{KWm^{-2}}$ obtained from simulations (ahead of flame front), the $B_i \approx 0.044$ and $\varphi \approx 0.31$ correspond to a thermally thin behavior of pine needle fuels. Hence, the solid chemical reaction time can be represented by the thermally thin kernel characteristic time τ_k [48], giving,

$$\tau_{react} = \tau_k = \frac{\rho_s C_{p,s}}{h_T \sigma_s} = 11.5 \sim 23\,\mathrm{s} \tag{6}$$

Where $\rho_s = 831.7\,\mathrm{kgm^{-3}}$ and $C_{p,s} = 2069.7\,\mathrm{Jkg^{-1}K^{-1}}$.

Following the above calculation where $\tau_{res} < \tau_{react}$, it is reasonable to retain a cold gauge, inert vegetation assumption because the vegetation has no time to adapt to the propagation of the flame front in a real case. Relevant parameters used for the above calculation and the below simulations are summarized in Table 1.

3. Results and discussion

3.1. Fire regime transition

To understand the effect of the configuration space $\{N_C, CdLAI\}$ on the fire regime transition, one important aspect might be to explore how does the configuration space change the flame tilt angle θ and whether the controlling mechanism using the configuration space can provide a better estimation of the tilt angle compared to previous models considering the role of N_C alone. Fig. 2 shows the role played by $CdLAI$ for a low wind speed case with $N_C = 20$. Increasing $CdLAI$ from 0.01 to 0.5 has clearly led to an increase of tilt angle from 52.7 to 70.94° representing the change of fire regime from plume-dominated to wind-driven. The tangent of the flame

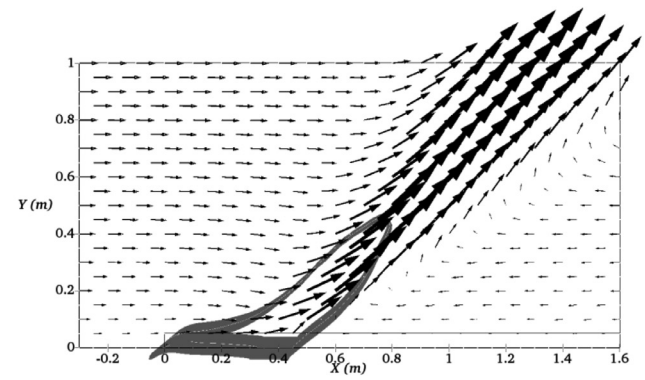

(a) $CdLAI = 0.01$, sparse vegetation.

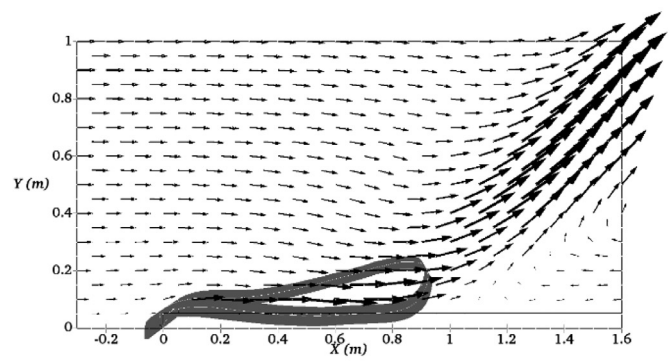

(b) $CdLAI = 0.5$, dense vegetation.

Fig. 2. The time-averaged velocity vector for $N_C = 20$ with length of arrow indicating velocity magnitude. Flame body (grey) is confined by $T = 500$ K.

tilt angle is defined as the ratio of flame width w_{flame} to the flame height H_{flame} given in Fig. 3.

Complete data points collected from prediction are shown in Fig. 4 for N_C ranging from 2 to 20 and $CdLAI$ ranging from 0.01 to 0.5. The chosen values for N_C and $CdLAI$ are based on two judgments: first, the fire data should cover two fire regimes [4], the plume-dominated $N_C > 10$ and wind-driven $N_C < 2$; second, the $CdLAI$ must cover the ABL to ML flame transition point at $CdLAI = 0.1$ [23] (see Section 1). Because it is observed that flame is completely wind-driven for $N_C = 2$ and the flame angle is hardly calculated due to irregular flame shape, no prediction for $N_C < 2$ is performed.

From Fig. 4a, it is observed that (a) for small N_C, the flame tilt angle is almost independent of $CdLAI$; (b) for small $CdLAI$ (sparse vegetation), flame tilt angle seems to be linearly proportional to N_C: the smaller the N_C, the larger the flame tilt angle corresponding to flame regime transition from plume-dominated to wind-driven; (c) the effect of large $CdLAI$ (dense vegetation) on changing flame tilt angle is non-ignorable for low wind speed, high N_C conditions that (d) the larger the $CdLAI$, the larger the flame tilt angle implying a tendency of the fire regime transition from plume-dominated to wind-driven.

Table 2
Two representative model correlations.

Eq.	Model correlations	Fuel	Ref.
(7)	$\tan(\theta) = C \times (\frac{2T_0}{T_f})^{1/5} \times Ka^{-1/5}$	Heptane, Ethanol, and Acetone	[50,51]
(8)	$\tan(\theta) = \begin{cases} C_1 \times \alpha^{1/2} N_C^{-1/3} & (N_C < 10) \\ C_2 \times \eta^2 N_C^{-2/3} & (N_C > 10) \end{cases}$	Long leaf pine, slash pine litter, *etc.*	[3]

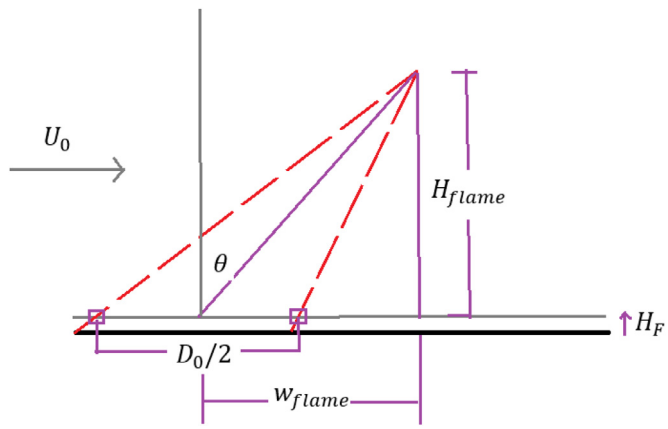

Fig. 3. Representation of flame tilt angle definition. Variables U_0, D_0, w_{flame}, H_{flame}, and H_F represent wind speed, flame depth, flame width, flame height, and vegetation height respectively.

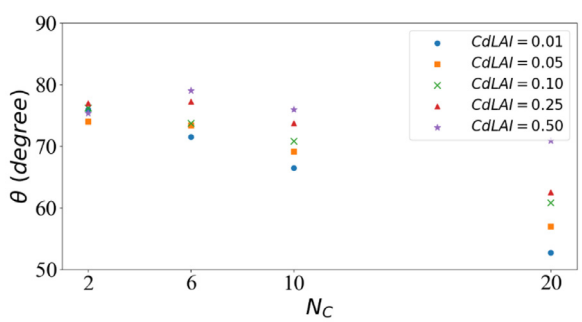

(a) θ vs. N_C

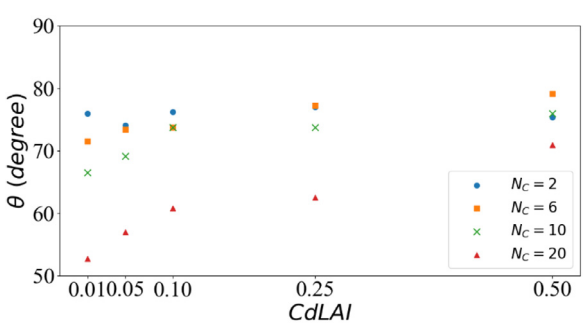

(b) θ vs. *CdLAI*

Fig. 4. The predicted flame tilt angle θ for different N_C and *CdLAI*.

From Fig. 4b, it seems that other than the data points for $N_C = 2$, flame tilt angle changes exponentially with *CdLAI, i.e.*, $\theta \sim e^{CdLAI}$. For $N_C = 2$, there is little effect of *CdLAI* on changing the flame tilt angle.

Lam and Weckman [49] reviewed several tilt angle model correlations for pool fire and wildland fire, the inner relationships for 13 models were examined and reason for different behaviors of these models were highlighted. Based on that study, Table 2 lists two representative model correlations proposed recently with the equation (8) not discussed in [49].

Table 3
A summary of parameters used to calculate flame tilt angle.

ρ_0 (kgm^{-3})	$C_{p,0}$ (Jkg^{-1}K^{-1})	T_0 (K)	T_f (K)	D (m)	I (KW)
1.19	1000	295	1000	0.5	100
U_0 (ms^{-1})	N_C	R_i	K_a	$K_a^{-1/5}$	$N_C^{-1/3}$
0.65356	20	8.0875	161.75	0.3616	0.368
0.8234	10	5.0952	50.952	0.4556	0.464
0.97629	6	3.6243	21.7458	0.54	0.55
1.408	2	1.7425	3.485	0.779	0.7937

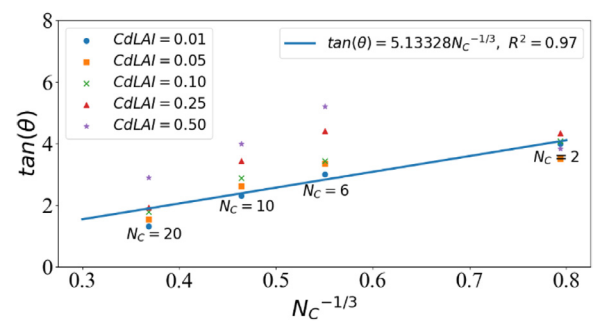

Fig. 5. The predicted flame tilt angle *vs.* $N_C^{-1/3}$ for different *CdLAI*.

The Equation (7) was originally defined by Hu et al. [51], given as,

$$\tan(\theta) = C \times \left[\frac{\rho_0 C_{p,0} \Delta T_f}{\dot{m}'' D^2 \Delta H_C} \times \left(\frac{T_0}{g \Delta T_f} \right)^2 \right]^{1/5} \tag{9}$$

Considering the fireline intensity $I = \dot{m}'' \Delta H_C D$, Byram convective number $N_C = 2gI/(\rho_0 U_0^3 C_{p,0} T_0)$, Richardson number $R_i = g\Delta T_f D / T_f U_0^2$, and assuming $K_a = N_C \times R_i$, Eq. (9) can be simplified to,

$$\begin{aligned} \tan(\theta) &= C \times \left[2 \times \frac{\rho_0 C_{p,0} T_0 U_0^3}{2gI} \times \frac{U_0^2 T_f}{g(T_f - T_0)D} \times \frac{T_0}{T_f} \right]^{1/5} \\ &= C \times \left(\frac{2T_0}{T_f} \right)^{1/5} \times [K_a]^{-1/5} \end{aligned} \tag{10}$$

Table 3 provides a summary of the properties used to calculate θ, N_C, R_i, K_a and their exponential values. Surprisingly, it is seen that the $K_a^{-1/5}$ and $N_C^{-1/3}$ share almost the same value indicating that Equation (7) may only be suitable for $N_C < 10$. Indeed, after careful examination of the experimental data in [51], the present authors notice that the flame tilt angles predicted with Equation (7) deviate from experimental tilt angles mainly for large N_C values (the N_C is about 800 for inaccurate fittings).

Nevertheless, Fig. 5 shows a plot for the predicted flame angles *vs* $N_C^{-1/3}$. A good agreement between the model correlation and predicted data can be clearly observed for $CdLAI = 0.01$, $N_C < 10$. Because of the similarity between $N_C^{-1/3}$ and $K_a^{-1/5}$, this has also evidenced the effectiveness of the model correlation proposed by Hu et al. [51]. The constant C in Equation (7) for heptane and ethanol was 9.1 [51], and the value for acetone was 4.16 [50]. In

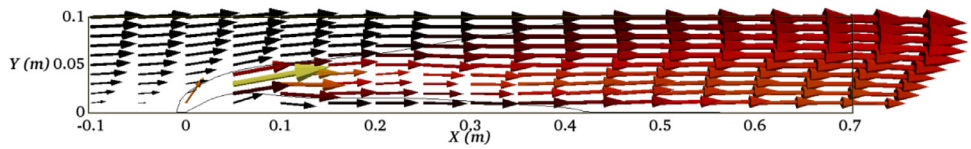

(a) $CdLAI = 0.01, N_C = 2$

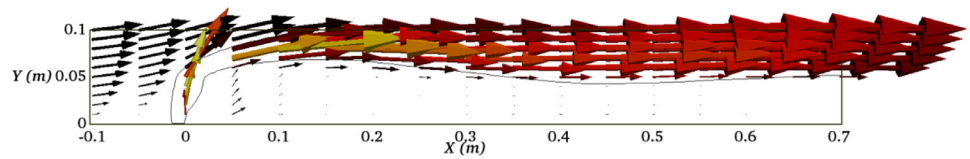

(b) $CdLAI = 0.5, N_C = 2$

Fig. 6. The velocity vectors close to the vegetation height $H_F = 0.05$ m; Length of arrow indicates velocity magnitude.

the present study, this constant is roughly 5.70. From the derivation of Equation (8) by Nelson et al. [3], the different values of that constant might be a result of different fraction of the impinging air entering the flame partially affected by the drag force from the vegetation and the pool [49]. Despite the relative effectiveness of the $N_C^{-1/3}$ and $K_a^{-1/5}$ correlations for low *CdLAI*, the effect of high *CdLAI* on flame tilt angle was essentially not considered by any of the available models in the past.

Besides, Fig. 5 has also shown that when wind speed is large corresponding to $N_C = 2$, the effect of *CdLAI* on changing flame tilt angle is small as observed in Fig. 4a. This is not because the *CdLAI* has no effect on changing the wind profile in the vegetation layer considering the wind is very strong but is because of the full entrainment of air into the flame above the vegetation (see Fig. 6). In other words, for $N_C = 2$, the effect of ML flow in the vegetation on flame behavior is negligible compared to that of the rapid development of ABL flow above the vegetation ($H_F = 0.05m$).

Because of the difficulty to consider the data points at $N_C = 2$, the Equation (8) is further examined for $N_C > 10$. According to Nelson et al. [3], the model correlation was built upon the consideration of the competing effect between the drag force $F_d \sim C_d \rho_0 U_e^2 HL$ and the buoyancy force $F_b \sim \rho w_0^2 HL$ where the C_d is the drag coefficient for the inclined flame and the $\eta = U_e/U_0$ represents the fraction of the impinging air entering the flame. The involvement of C_d and η provides a good starting point to consider the role of *CdLAI*. From Fig. 6, it is very obvious that the role of *CdLAI* is to suppress the sub-layer flow while improve the air entrainment above the vegetation. Because η is defined for the fraction of impinging air above the vegetation, it is reasonable to write $\eta \sim CdLAI$. While, considering that only the natural log part of the entrained air participates in the combustion due to the log wind profile given in Eq. (1), the correlation may be further written as $ln\eta \sim CdLAI$, giving,

$$ln\eta = C_1 CdLAI \text{ or } \eta = e^{(C_1 CdLAI)} \tag{11}$$

The entrainment velocity is then written as,

$$U_e = e^{(C_1 CdLAI)} U_0 \tag{12}$$

The tangent of the flame tilt angle is the ratio of drag force to buoyancy force,

$$\tan(\theta) = \frac{F_d}{F_b} \sim \frac{\rho_0 U_e^2 HL}{\rho w_0^2 HL} = \frac{\rho_0 e^{(2C_1 CdLAI)} U_0^2 HL}{\rho w_0^2 HL} = \frac{\rho_0}{\rho} \times e^{2C_1 CdLAI} \times N_C^{-2/3} = C_2 e^{2C_1 CdLAI} \times N_C^{-2/3} \tag{13}$$

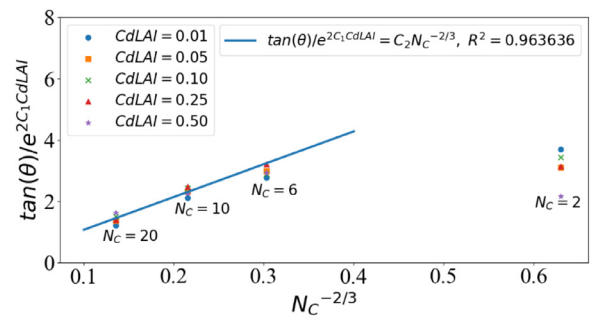

Fig. 7. The best fit model correlation for different N_C and *CdLAI*.

Where $U_0/w_0 = N_C^{-1/3}$ because the characteristic buoyancy velocity w_0 [52] can be written as,

$$w_0 = \left(\frac{2gI}{\rho_0 C_{p,0} T_0}\right)^{1/3} \text{ and } N_C = \frac{2gI}{\rho_0 C_{p,0} T_0 U_0^3} \tag{14}$$

The Eq. (13) is then used to fit the predicted flame tilt angle data for $N_C = 6$, 10 and 20 though the equation seems to work only for $N_C > 10$. The comparison between the best fit equation with the constants $C_1 = 0.5366287$, $C_2 = 10.76685369$ and the collapsed data is shown in Fig. 7. A good matching is obtained for $N_C > 10$, while predicted data slightly deviate from that predicted using the model Eq. (13) for $N_C = 6$ and the model fails for $N_C = 2$. In fact, our previous study [35] showed that the flame regime transition from plume-dominated to wind-driven occurs roughly at $N_C = 5.6$ by observing the flame shapes for the case of $CdLAI = 0.01$. It is therefore concluded that the proposed model Equation (7) works primarily for plume-dominated fire.

The model correlation $\tan(\theta) = 10.76685369 e^{1.0732574 CdLAI} \times N_C^{-2/3}$ is, in some extent, agrees well with the findings from Fig. 4b that $\theta \sim e^{CdLAI}$.

3.2. Radiative heat power

The effect of the configuration space {N_C, *CdLAI*} on the radiative heat power to the unburnt vegetation layer in front of the fire front is demonstrated in Fig. 8. The radiative heat power is defined as the *CdLAI* weighted total radiation written as $P_{rad} = \int Q_{rad}^s dv/CdLAI$. The chosen of the radiative heat power is for the purpose of considering the in-depth radiation effect caused by the characteristic of vegetation, *i.e.*, the *CdLAI*.

From Fig. 8, it is found that (a) the effect of *CdLAI* on radiative heat power is large for both plume-dominated and wind-driven

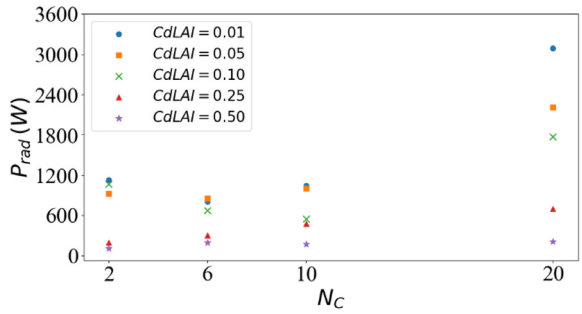

(a) Radiative heat power P_{rad} vs. N_C

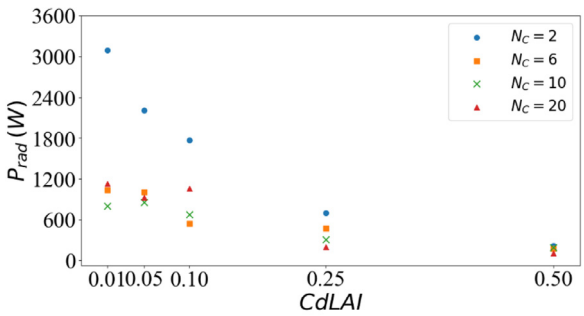

(b) Radiative heat power P_{rad} vs. $CdLAI$

Fig. 8. The predicted radiative heat power P_{rad} for different N_C and *CdLAI*.

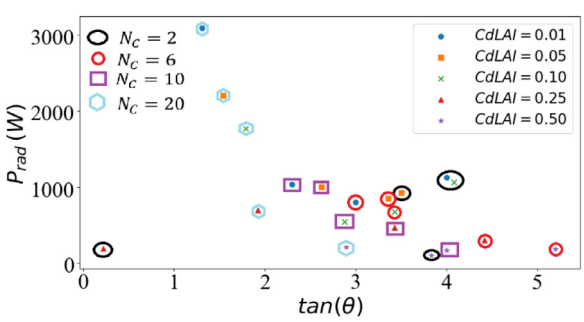

Fig. 9. The predicted radiative heat powerP_{rad} *vs.* tanθ for different N_C and *CdLAI*.

fires, while its effect is small for transitional fire roughly at $N_C = 6$ (or 5.6 from a previous study [35]); (b) wind (or N_C) has little effect on radiative heat power for large *CdLAI*, while it plays an important role when vegetation is sparse ($CdLAI = 0.01$); (c) excluding the data points for $N_C = 2$, there seems to exist a relationship between P_{rad} and the proposed configuration space, *i.e.* $P_{rad} \sim f(N_C, CdLAI)$.

To correlate the configuration space with the radiative heat power, the first step might be to consider the effect of flame tilt angle θ on the radiative heat power P_{rad}. Fig. 9 is hence provided in order to correlate these quantities. Because a model correlation has been proposed for the tangent of the tilt angle θ and the configuration space $\{N_C, CdLAI\}$, $tan(\theta)$ rather than θ is considered in the figure. The proposed model is again given as,

$$\tan(\theta) = 10.76685369e^{1.0732574CdLAI} \times N_C^{-2/3} \tag{15}$$

A good fitting of Eq. (15) with the predicted data was obtained for $N_C > 10$, while data slightly deviated from the prediction for $N_C = 6$ and the model failed for $N_C = 2$. Indeed, from Fig. 9, the black color circled data points for $N_C = 2$ are far from the main trend of the other points that a best fit model proposed excluding

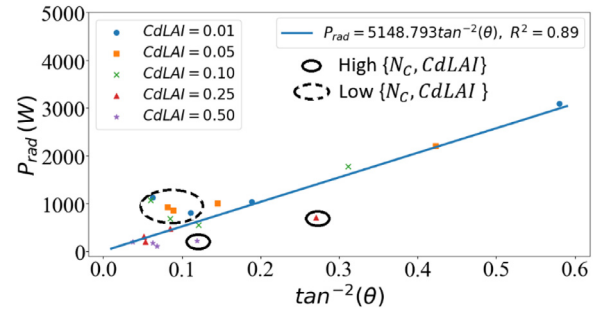

Fig. 10. The fitting curve of the radiative heat power P_{rad} *vs.* tan$^{-2}\theta$ for different N_C and *CdLAI*.

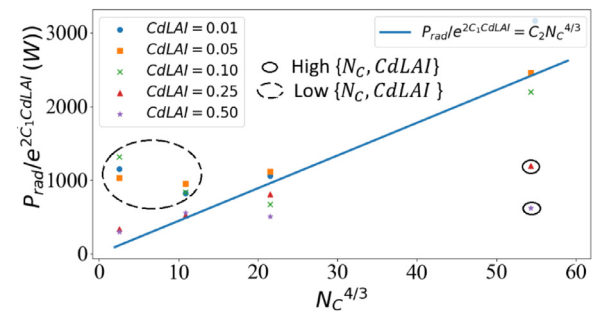

Fig. 11. The best fit model correlation for different N_C and *CdLAI*.

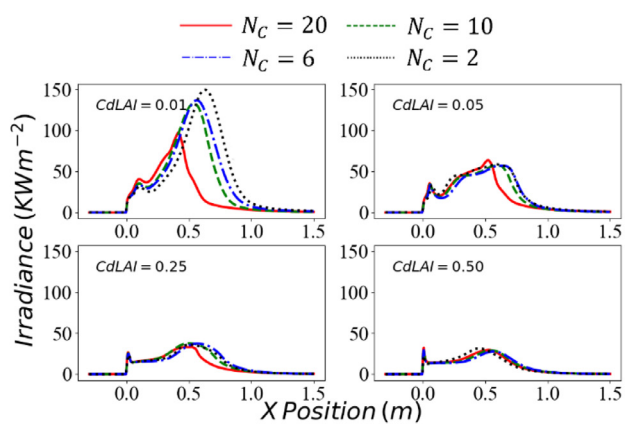

(a)

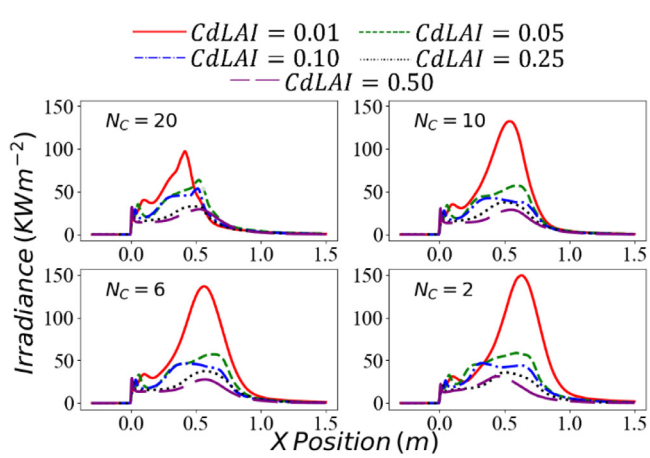

(b)

Fig. 12. Irradiance or radiative heat flux on the vegetation surface.

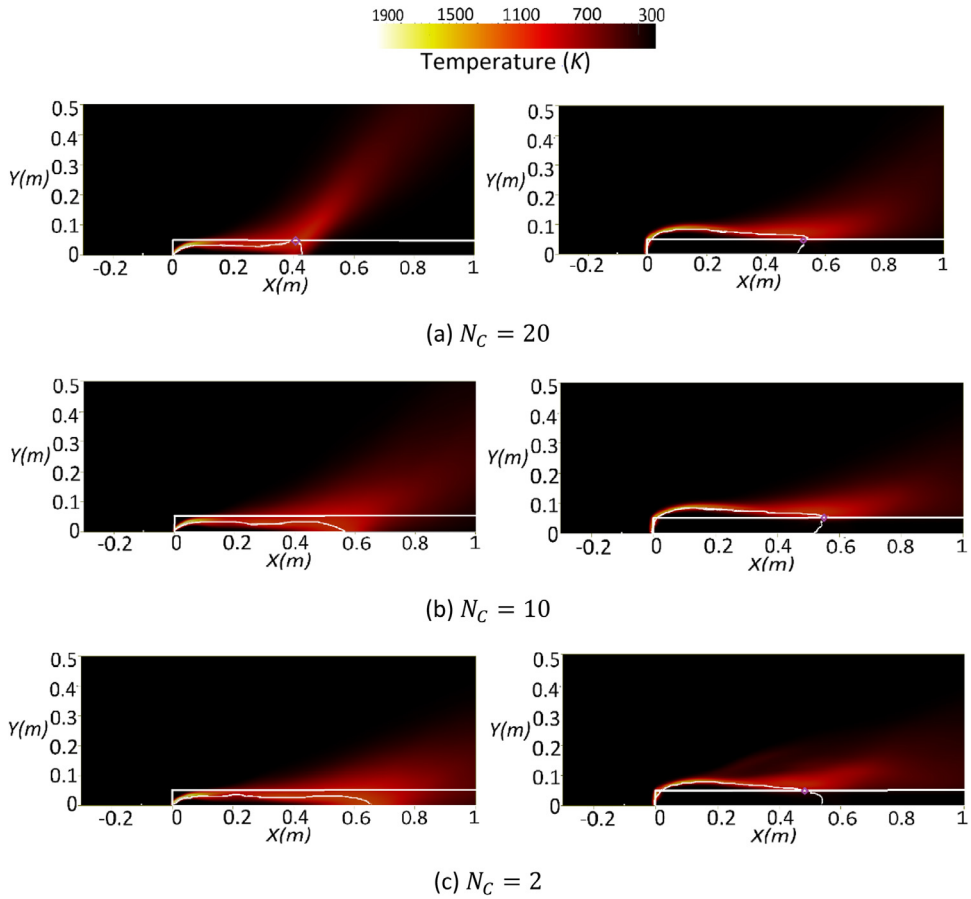

Fig. 13. Temperature contours for different N_C and $CdLAI$. Left: $CdLAI = 0.01$; Right: $CdLAI = 0.5$.

those points is given as,

$$P_{rad} = 5148.793\tan^{-2}(\theta) \text{ with } R^2 = 0.89 \tag{16}$$

The fitting curve is then given separately in Fig. 10 for clarity. It is noteworthy that the model correlation does not fit the data mainly for the cases of high $\{N_C, CdLAI\}$ and low $\{N_C, CdLAI\}$ representing the two extreme conditions: the {low wind speed, dense vegetation} and the {high wind speed, sparse vegetation}. These observations might becaused by the assumption of a constant χ_{rad}, the ratio of thermal radiation to the theoretical heat release rate, which is more influenced by the two extreme conditions. A proper calibration of $\chi_{rad} \sim f(N_C, CdLAI)$ from experiments may provide more accurate mathematical correlations since the value of χ_{rad} changes for the combustion of different fluid/solid fuel type at different conditions [53,54].

Consequently, substituting Eq. (15) into Eq. (16) leads to the relationship between P_{rad} and $\{N_C, CdLAI\}$ given as,

$$P_{rad} = C_2 e^{2C_1 CdLAI} N_C^{4/3} \tag{17}$$

With $C_1 = -1.0732574$ and $C_2 = 44.41481$ following the format of the derived equation (7).

Indeed, this model correlation $P_{rad} \sim f(N_C^{4/3}, CdLAI)$ is not far from the observation in Fig. 8 that $P_{rad} \sim f(N_C, CdLAI)$. The fitting curve is then shown in Fig. 11 with completely wrong fittings for the cases in extreme conditions due to amplified error from substitution. For moderate $\{N_C, CdLAI\}$, good fitting is obtained.

3.3. Radiative heat flux and general behaviors

Other than discussing the behavior of the radiative heat power to the entire vegetation layers ahead of the flame front, the radiative heat flux or the irradiance J on the top surface of the vegetation is presented in Fig. 12. From Fig. 12a, it is observed that N_C has a strong influence on the radiative heat flux across the sparse vegetation surface ($CdLAI = 0.01$), while its effect rapidly decreases for denser vegetation ($CdLAI = 0.5$). The minimal effect of N_C for the case of $CdLAI = 0.5$ leads to the overlapping of the curves implying that N_C alone can be used to predict radiative heat flux from flame body to the majority types of the forest fuel layers as it was reported that the most forest fuel layers such as needles or shrubs exhibit $CdLAI > 0.5$ [13,55]. Moreover, it was widely accepted that N_C may be used independently to classify the fire regime transition defined by the ratio of radiative to convective heat transfer. For $CdLAI = 0.5$ in Fig. 12a which is a typical case for forest fire study, the little effect of N_C on the radiative heat flux indicates that the N_C is mainly responsible for changing convective heat transfer to the vegetation, and therefore changing the ratio of radiative to convective heat transfer. For $CdLAI < 0.5$ often for small scale litter fires, both radiative and convective heat transfer are influenced by N_C.

On the other hand, Fig. 12b explicitly demonstrates the effect of $CdLAI$ on the radiative heat flux across unburnt vegetation under different wind conditions. For $N_C = 20$ representing low wind power, increasing $CdLAI$ leads to the shift of the peak irradiance to the right (downstream); while as N_C decreases, this observation is reversed that the peak irradiance shifts more to the left (upstream) following the decrease of N_C from 10 to 2. It might be interesting to know what do the peaks represent and does it in some extent relate to the validity of the model correlations proposed in Sections 3.1 and 3.2. A first implication is that the position of the peaks is a result of local heat release rate within the flame body, and hence it may also be related to the stochiometric

fuel/air ratio and further the fraction of impinging air entering the flame.

Fig. 13 shows the temperature contour plots of the fires. The stochiometric fuel/air ratio and the vegetation are labeled with the white solid line. The former one has an irregular shape and is referred to as a stochiometric line in the following discussion, and the latter one has a rectangular shape with the top sitting at $Y = H_F = 0.05$ m. Interestingly, the intersection points between the stochiometric line and the vegetation top reflect almost exactly the position of the irradiance peaks observed in Fig. 12.

However, it is also noticed that the stochiometric line cannot always go beyond the surface top that for cases such as $\{N_C = 6,\ CdLAI = 0.01\}$ and $\{N_C = 2,\ CdLAI = 0.01\}$, no intersection points can be observed. These configuration spaces are the low $\{N_C,\ CdLAI\}$ cases discussed in Figs. 10 and 11 where most inaccurate fittings were found. Practically speaking, whether the stochiometric line can go beyond the vegetation surface or not relates strictly with the fraction of impinging air into the flame. Because the fraction of entrainment within the vegetation layer is not considered into the model correlation of Eq. (17) due to the fact that the equation inherits the features of Eq. (15) for the flame tilt angle defined above the vegetation, the above observation has essentially explained why the two proposed mode correlations does not fit all available fire data.

4. Conclusion

This study was motivated by the lack of knowledge on how does vegetation characteristic (defined as *CdLAI* in the present study) may affect the small-scale fire regime transition and heat transfer mechanism. Previous studies have highlighted the role of Byram convective number N_C on describing the behavior of 'free' fires, *i.e.*, fires without vegetation around (for pool fire) or without vegetation property distinguished (for wildland fire) [4,6], the responsibility of vegetation property on fire behavior were hence remain unclear. The flame models established based on these fires may result in inaccurate large- and giga-scale fire modeling due to wrong 'prior' flame shape estimated from θ ~ wind speed [56]. An accurate flame model considering the role of vegetation characteristics is essential to extend the limit of validity of large-scale fire models. Therefore, the present work first discussed the non-ignorable effect of the vegetation characteristics on the flame tilt angle and the radiative heat transfer, and then proposed new model correlations for predicting these two quantities using a configuration space $\{N_C, CdLAI\}$. The main results are summarized as follows:

- Two previous experimental based flame tilt angle models by Hu et al. [51] and Nelson et al. [3] are found to have similar performance for $N_C < 10$. For $N_C > 10$, the model correlation by Nelson et al. fits with the predicted flame tilt angle mainly for small *CdLAI*. Neither of the models can be extensively used for different types of vegetation characteristics due to lack of considering *CdLAI*.
- For $N_C > 6$, a new flame tilt angle model is proposed as $\tan(\theta) = C_2 e^{2C_1 CdLAI} \times N_C^{-2/3}$ with C_1 being positive, *i.e.*, flame tilt angle is directly related to *CdLAI* while inversely related to N_C.
- A new model for radiative heat power reaching the vegetation ahead of the flame front is proposed as $P_{rad} = C_2 e^{2C_1 CdLAI} N_C^{4/3}$ with C_1 being negative, *i.e.*, radiative heat power is reversely related to *CdLAI* while directly related to N_C.
- The radiation model is valid for moderate $\{N_C, CdLAI\}$ primarily due to the role of *CdLAI* on changing the fraction of impinging air into the flame above the vegetation layer, and may also be a result of the constant χ_{rad} used for prediction.
- Overall, the present work showed the importance of considering the vegetation characteristic in the flame models that the proposed model correlations based on the configuration space $\{N_C, CdLAI\}$ should be used for large- or giga-scale flame modeling instead of the more classical free fire model correlations.

Declaration of Competing Interest

None declared.

CRediT authorship contribution statement

Kai Zhang: Conceptualization, Methodology, Formal analysis, Writing - original draft, Writing - review & editing. **Aymeric Lamorlette:** Writing - review & editing, Supervision, Project administration.

Acknowledgments

This work is supported by Labex MEC (ANR-10-LABX-0092) and the A*MIDEX project (ANR-11-IDEX-0001-02), funded by the "Investissements d'Avenir".

This work was granted access to the HPC resources of Aix-Marseille University financed by the project Equip@Meso (ANR-10-EQPX-29-01) of the program "Investissements d'Avenir" supervised by the Agence Nationale pour la Recherche.

References

[1] A.L. Sullivan, Wildland surface fire spread modelling, 1990–2007. 1: physical and quasi-physical models, Int. J. Wildl. Fire 18 (2009) 349–368.
[2] P.J. Pagni, T.G. Peterson, Flame spread through porous fuels, Symp. (Int.) Combust. 14 (1983) 1099–1107.
[3] R.M. Nelson, B.W. Butler, D.R. Weise, Entrainment regimes and flame characteristics of wildland fires, Int. J. Wildl. Fire 21 (2012) 127–140.
[4] R.M. Nelson, *Re*-analysis of wind and slope effects on flame characteristics of Mediterranean shrub fires, Int. J. Wildl. Fire 24 (2015) 1001–1007.
[5] F. Morandini, X. Silvani, Experimental investigation of the physical mechanisms governing the spread of wildfires, Int. J. Wildl. Fire 19 (2010) 570–582.
[6] D. Morvan, N. Frangieh, Wildland fires behaviour: wind effect *versus* Byram's convective number and consequences upon the regime of propagation, Int. J. Wildl. Fire 27 (2018) 636–641.
[7] D. Morvan, J.L. Dupuy, Modeling the propagation of a wildfire through a Mediterranean shrub using a multiphase formulation, Combust. Flame 138 (2004) 199–210.
[8] A.L. Sullivan, Convective Froude number and Byram's energy criterion of Australian experimental grassland fires, Proc. Combust. Inst. 31 (2007) 2557–2564.
[9] D. Morvan, S. Meradji, G. Accary, Physical modelling of fire spread in grasslands, Fire Saf. J. 44 (2009) 50–61.
[10] D. Morvan, Physical phenomena and length scales governing the behaviour of wildfires: a case for physical modelling, Fire Technol. 47 (2011) 437–460.
[11] N. Frangieh, D. Morvan, S. Meradji, G. Accary, O. Bessonov, Numerical simulation of grassland fires behavior using an implicit physical multiphase model, Fire Saf. J. 102 (2018) 37–47.
[12] S. Verma, A. Trouve, A study of the structure of a turbulent line fire subjected to cross-flow using large eddy simulations, in: Proceedings of the 8th International Conference on Forest Fire Research, 2018, pp. 319–324.
[13] A. Lamorlette, M.E. Houssami, J.C. Thomas, A. Simeoni, D. Morvan, A dimensional analysis of forest fuel layer ignition model: application to the ignition of pine needle litters, J. Fire Sci. 33 (2015) 320–335.
[14] B. Benkoussas, J.L. Consalvi, B. Porterie, N. Sardoy, J.C. Loraud, Modelling thermal degradation of woody fuel particles, Int. J. Thermal Sci. 46 (2007) 319–327.
[15] H.M. Nepf, turbulence Drag, and diffusion in flow through emergent vegetation, Water Resour. Res. 35 (1999) 479–489.
[16] C.H.K. Williamson, The natural and forced formation of spot-like 'vortex dislocations' in the transition of a wake, J. Fluid Mech. 243 (1992) 393–441.
[17] J.L. Dupuy, M. Larini, Fire spread through a porous forest fuel bed: a radiative and convective model including fire-induced flow effects, Int. J. Wildl. Fire 9 (1999) 155–172.
[18] F. Morandini, Y. Perez-Ramirez, V. Tihay, P.A. Santoni, T. Barboni, Radiant, convective and heat release characterization of vegetation fire, Int. J. Thermal Sci. 70 (2013) 83–91.
[19] E. Pastor, L. Zárate, E. Planas, J. Arnaldos, Mathematical models and calculation systems for the study of wildland fire behaviour, Prog. Energy Combust. Sci. 29 (2003) 139–153.
[20] N. Luminari, C. Airiau, A. Bottaro, Drag-model sensitivity of Kelvin-Helmholtz waves in canopy flows, Phys. Fluids 28 (2016) 124103.

[21] M.R. Raupach, A.S. Thom, Turbulence in and above plant canopies, Annu. Rev. Fluid Mech. 13 (1981) 97–129.
[22] J. Finnigan, Turbulence in plant canopies, Annu. Rev. Fluid Mech. 32 (2000) 519–571.
[23] M. Ghisalberti, H. Nepf, The structure of the shear layer in flows over rigid and flexible canopies, Environ. Fluid Mech. 6 (2006) 277–301.
[24] R. Sun, S.K. Krueger, M.A. Jenkins, M.A. Zulauf, J.J. Charney, The importance of fire–atmosphere coupling and boundary-layer turbulence to wildfire spread, Int. J. Wildl. Fire 18 (2009) 50–60.
[25] D. Morvan, A. Lamorlette, Impact of solid fuel particle size upon the propagation of a surface fire through a homogeneous vegetation layer, Fire Saf. Sci. 11 (2014) 1326–1338.
[26] M. El Houssami, A. Lamorlette, D. Morvan, R.M. Hadden, A. Simeoni, Framework for submodel improvement in wildfire modelling, Combust. Flame 190 (2018) 12–24.
[27] M. El Houssami, J.C. Thomas, A. Lamorlette, D. Morvan, M. Chaos, R. Hadden, A. Simeoni, Experimental and numerical studies characterizing the burning dynamics of wildland fuels, Combust. Flame 168 (2016) 113–126.
[28] B.F. Magnussen, B.H. Hjertager, On mathematical modeling of turbulent combustion with special emphasis on soot formation and combustion, Symp. (Int.) Combust. 16 (1977) 719–729.
[29] F. Nicoud, F. Ducros, Subgrid-scale stress modelling based on the square of the velocity gradient tensor, Flow, Turbul. Combust. 62 (1999) 183–200.
[30] L. Liang, L. Xiaofeng, L. Borong, Z. Yingxin, Improved k–ε two-equation turbulence model for canopy flow, Atmos. Environ. 40 (2006) 762–770.
[31] R. Siegel, J.R. Howell, Thermal Radiation Heat Transfer, Hemisphere Publishing Corporation, Washington DC, 1992.
[32] N.J. De Mestre, E.A. Catchpole, D.H. Anderson, R.C. Rothermel, Uniform propagation of a planar fire front without wind, Combust. Sci. Technol. 65 (1989) 231–244.
[33] R.R. Linn, J.M. Canfield, P. Cunningham, C. Edminster, J.L. Dupuy, F. Pimont, Using periodic line fires to gain a new perspective on multi-dimensional aspects of forward fire spread, Agric. For. Meteorol. 157 (2012) 60–76.
[34] M.A. Finney, J.D. Cohen, J.M. Forthofer, S.S. McAllister, M.J. Gollner, D.J. Gorham, K. Saito, N.K. Akafuah, B.A. Adam, J.D. English, Role of buoyant flame dynamics in wildfire spread, Proc. Natl. Acad. Sci. 112 (2015) 9833–9838.
[35] K. Zhang, S. Verma, A. Trouve, A. Lamorlette, A study of the canopy effect on fire regime transition using an objectively defined Byram convective number, Fire Saf. J. (2020) 102950.
[36] N.P. Cheney, J.S. Gould, W.R. Catchpole, Prediction of fire spread in grasslands, Int. J. Wildl. Fire 8 (1998) 1–13.
[37] D. Morvan, Wind, effects, unsteady behaviors, and regimes of propagation of surface fires in open field, Combust. Sci. Technol. 186 (2014) 869–888.
[38] S. Patankar, Numerical Heat Transfer and Fluid Flow, CRC press, 1980.
[39] P.J. DiNenno, SFPE Handbook of Fire Protection Engineering, SFPE, 2008.
[40] D. Morvan, J.L. Dupuy, Modeling of fire spread through a forest fuel bed using a multiphase formulation, Combust. Flame 127 (2001) 1981–1994.
[41] W. Mell, A. Maranghides, R. McDermott, S.L. Manzello, Numerical simulation and experiments of burning douglas fir trees, Combust. Flame 156 (2009) 2023–2041.
[42] D. Cancellieri, V. Leroy-Cancellieri, E. Leoni, Multi-scale kinetic model for forest fuel degradation, 7th International Conference on Forest Fire Research, 2014.
[43] N.D. Burrows, Flame residence times and rates of weight loss of eucalypt forest fuel particles, Int. J. Wildl. Fire 10 (2001) 137–143.
[44] A. Lamorlette, F. Candelier, Thermal behavior of solid particles at ignition: theoretical limit between thermally thick and thin solids, Int. J. Heat Mass Transf. 82 (2015) 117–122.
[45] A.M. Grishin, Mathematical Modeling of Forest Fires and New Methods of Fighting them, Publishing house of the Tomsk state university, 1997.
[46] R.T. Long, J.L. Torero, J.G. Quintiere, A.C. Fernandez-Pello, Scale and transport considerations on piloted ignition of PMMA, Fire Saf. Sci. 6 (2000) 567–578.
[47] A. Simeoni, J.C. Thomas, P. Bartoli, P. Borowieck, P. Reszka, F. Colella, P.A. Santoni, J.L. Torero, Flammability studies for wildland and wildland–urban interface fires applied to pine needles and solid polymers, Fire Saf. J. 54 (2012) 203–217.
[48] A. Lamorlette, Quantification of ignition time uncertainty based on the classical ignition theory and Fourier analysis, Comptes Rendus Mécanique 342 (2014) 459–465.
[49] C.S. Lam, E.J. Weckman, Wind-blown pool fire, Part II: comparison of measured flame geometry with semi-empirical correlations, Fire Saf. J. 78 (2015) 130–141.
[50] F. Tang, L.J. Li, K.J. Zhu, Z.W. Qiu, C.F. Tao, Experimental study and global correlation on burning rates and flame tilt characteristics of acetone pool fires under cross air flow, Int. J. Heat Mass Transf. 87 (2015) 369–375.
[51] L. Hu, S. Liu, J.L. de Ris, L. Wu, A new mathematical quantification of wind-blown flame tilt angle of hydrocarbon pool fires with a new global correlation model, Fuel 106 (2013) 730–736.
[52] R.M. Nelson Jr, Power of the fire—A thermodynamic analysis, Int. J. Wildl. Fire 12 (2003) 51–65.
[53] R.G. Zalosh, Industrial Fire Protection Engineering, Wiley, Hoboken, NJ, 2003.
[54] L. Hu, F. Tang, Q. Wang, Z. Qiu, Burning characteristics of conduction-controlled rectangular hydrocarbon pool fires in a reduced pressure atmosphere at high altitude in Tibet, Fuel 111 (2013) 298–304.
[55] N.P. Cheney, J.S. Gould, W.R. Catchpole, The influence of fuel, weather and fire shape variables on fire-spread in grasslands, Int. J. Wildl. Fire 3 (1993) 31–44.
[56] O. Séro-Guillaume, S. Ramezani, J. Margerit, D. Calogine, On large scale forest fires propagation models, Int. J. Thermal Sci. 47 (2008) 680–694.